# Dynamic Improvement of Inductive Power Transfer Systems With Maximum Energy Efficiency Tracking Using Model Predictive Control: Analysis and Experimental Verification

Shunpan Liu, Ruikun Mai, *Member, IEEE*, Lingyun Zhou, Yong Li, *Member, IEEE*, Jiefeng Hu, *Senior Member, IEEE*, Zhengyou He, *Senior Member, IEEE*, Zhaotian Yan, and Shiqi Wang

***Abstract*—For inductive power transfer (IPT) systems, loads and system input voltages are subject to change, which affects system efficiency and stability. This article presents a perturbation and observation (P&O) method for maximum energy efficiency tracking (MEET) with a model predictive control (MPC) scheme for improving the dynamic performance of series–series compensated IPT systems. In the IPT system, the inverter at the primary side incorporates the P&O method and phase shift modulation (PSM) to minimize system input power. Meanwhile, the rectifier at the secondary side is controlled by MPC control based PSM to improve the dynamic response of the output voltage. Simulated and experimental results show that, compared to the PI controller, the MPC controller, based on a simple but accurate mathematical model, has a better dynamic response to load and input voltage variations. With the MPC controller, the settling time of the output voltage is reduced by 85.7%, which indicates a particularly stable power supply to the load. Furthermore, MEET adopting the P&O method in the IPT system can promote the system efficiency by 1.85% on average when the output voltage is regulated by the MPC controller.**

***Index Terms*—Dynamic mathematical model, inductive power transfer (IPT), maximum energy efficiency tracking (MEET), model predictive control (MPC), perturbation and observation (P&O).**

Manuscript received December 17, 2019; revised March 16, 2020; accepted April 20, 2020. Date of publication May 3, 2020; date of current version July 31, 2020. This work was supported in part by the National Key Research and Development Program of China under Grant 2017YFB1201002, in part by the National Natural Science Foundation of China under Grants 51907169, 51977184, and 51677155, in part by the International Science and Technology Innovation Cooperation Program of Sichuan Province under Grant 2020YFH0031, and in part by the Fundamental Research Funds for the Central Universities under Grant 2682020CX16. Recommended for publication by Associate Editor A. Safaee. *(Corresponding author: Ruikun Mai.)*

Shunpan Liu, Ruikun Mai, Lingyun Zhou, Yong Li, Zhengyou He, Zhaotian Yan, and Shiqi Wang are with the School of Electrical Engineering, Southwest Jiaotong University, Chengdu 611756, China (e-mail: liusp@my.swjtu.edu.cn; mairk@swjtu.edu.cn; zhouly@my.swjtu.edu.cn; leeo1864@163.com; hezy@home.swjtu.edu.cn; zhaotian_yan@163.com; wsq34706@my.swjtu.edu.cn).

Jiefeng Hu is with the School of Science, Engineering and Information Technology, Federation University Australia, Mount Helen, Vic 3353, Australia (e-mail: j.hu@federation.edu.au).

Color versions of one or more of the figures in this article are available online at https://ieeexplore.ieee.org.

Digital Object Identifier 10.1109/TPEL.2020.2992517

## I. Introduction

INDUCTIVE power transfer (IPT) technology can transfer energy from power supplies to loads through electromagnetic coupling [1]–[4]. As a flexible and reliable contactless power supply approach, IPT technology effectively avoids electrical sparks, leakage and other safety problems that exist in plug-in systems [3]–[5]. With the rapid development of power electronics techniques, compensation networks design, and couplers design, IPT systems have already proved their high efficiency and reliability in the harsh environment. Over the last decade, this technology has been widely applied in many applications, such as smartphones [6], electric vehicles [7]–[10], and electric busses [11], [12].

Usually, an IPT system contains high-frequency converters, magnetic couplers, high-order compensation networks, and other nonlinear elements. The complex system structure and high operating frequency bring in difficulties in the effective control of IPT systems, especially during transients [13], [14]. For example, in dynamic IPT systems, coupling coefficient and equivalent load resistance vary when vehicles with receiver coils are moving [15]–[17]. Even in some stationary IPT systems, fluctuations of system input voltage and pulsed power loads are unavoidable. These issues may lead to a sharp decrease in system efficiency and continuous power oscillation.

To improve power transfer efficiency, some optimal methods are already adopted for IPT systems [18]–[22]. These methods can be classified into three main categories, i.e., operating frequency shifting, dynamic tuning, and equivalent impedance matching. Changing the operating frequency of the IPT system can regulate the equivalent load resistance and system output gain. Thus, higher efficiency can be achieved, especially in some small-volume applications with low mutual inductance [18]. However, the frequency bifurcation phenomenon may occur with variable load [23], and the inverter of IPT systems can hardly achieve zero phase angle [24]. Besides, dynamic tuning methods [19] are also good for improving system efficiency. These methods are designed to overcome the detuning of the IPT system caused by working temperature or aging of inductors and capacitors. Unfortunately, to dynamically tune the IPT system, it is unavoidable to increase the volume and complexity due to

necessary extra passive components and switches. In addition, dc–dc converters [20], inverters, and active rectifiers [21] of the IPT system are used for altering the load impedance. The power losses in coupled coils can be minimized, when converters are regulated to optimize the currents in the coils. However, these schemes always idealize passive components and ignore converter losses of the IPT system when calculating the optimal efficiency point. Thus, the optimal efficiency will not be actually activated.

In [22], maximum energy efficiency tracking (MEET) is achieved by searching for the minimum input power for inherent given output power. Here, hill-climbing-search, i.e., perturbation and observation (P&O) method is applied and performs accurate tracking of the maximum efficiency point. While the IPT system can operate in MEET with the cooperation of P&O method by regulating the inverter at the primary side, it performs poorly in dynamic responding to variations of the load resistance and the input voltage because of the PI controlled rectifier at the secondary side.

If the control scheme of the dynamic IPT system performs poorly in responding to dynamic variations of system parameters, unexpected long settling time and overshoot/ undershoot, which always indicates power oscillations, will occur. These frequent power oscillations of the IPT system will sharply reduce the equipment lifetime. Furthermore, poor system dynamic performance has a great drawback on overall efficiency and working conditions of motors, batteries, and other electrical equipment, while imposes additional requirements on volume and reliability of the whole system [25], [26].

To improve the dynamic performance of IPT systems, excellent controllers and their supporting control schemes for power converters in the IPT system are necessary. In the past few years, some optimized control schemes have been utilized to control power converters in the IPT system, such as optimal PI control [27] and sliding mode control (SMC) [28]. PI control is a typical linear control scheme with a simple mathematical model. By optimizing the controller design, better dynamic performance could be achieved. However, its dynamic performance is still limited by the inherent characteristics of the PI controller. Compared with the PI controller, the SMC scheme performs better in responding to step variations [28]. However, the modeling process of the SMC is more complicated, which increases the complexity of the controller.

Model predictive control (MPC) is a promising and advanced method for power converters. This scheme shows superior dynamic performances, and it provides corresponding cost functions for different topologies and different applications. The MPC controller can predict future behaviors of converters under different control variables by setting an accurate mathematical model. Then, the optimum control variable will be chosen to achieve system control objectives during the rolling calculation process [29]. Nowadays, owing to its excellent performance, MPC has been utilized in many power electronic applications, such as pulsewidth modulation rectifiers [30], grid-connected inverters [31], and induction motors drives [32].

Recently, MPC has also been proposed to achieve a superior performance of the IPT system [33], [34]. This controller offers a faster dynamic response than the PI control scheme while it has a simpler mathematical model compared with the SMC scheme. However, the scheme presented in [33] has not built a discrete dynamic system mathematical model, and the phase angles of the inverter and the rectifier are determined by direct power prediction without a feedback correction rather than by rolling calculation. As a result, the dynamic performance of the controller is affected. In [34], the MPC scheme is adopted to cooperate with pulse density modulation. With rolling calculation for voltage prediction and cost function optimization, a better dynamic response is achieved. Unfortunately, the maximum efficiency point in [34] is also determined by minimizing the power loss in coils, and the power losses of converters are ignore, which produces more possibilities for mismatching of the control signals between the calculation results and the optimum values.

To ensure the dynamic performance of the system, a simple but accurate discrete mathematical model of the IPT system is highly desired to cooperate with the MPC scheme to shorten the calculation time of the microcontroller unit. Some dynamic modeling methods, such as coupled modes, small-signal modeling, and generalized state-space averaging method have been investigated [35]–[39]. However, the IPT system is a high-order and nonlinear system, which makes the calculating process of the modeling methods above time-consuming.

In summary, few research works have realized MEET in the IPT system. However, while MEET is actually achieved, the dynamic response of the IPT system needs to be further improved by an excellent control scheme with a simple and accurate discrete mathematical model. Thus, most of the unexpected transient phenomena, such as power oscillations and overshoot, can be reduced or avoided. The contributions of this article are listed as follows.

1) To provide a reliable and simple calculation basis for the controller of the IPT system, a dynamic mathematical model of the series–series (SS) compensated IPT system, based on the active rectifier modeling and phase shift modulation (PSM), is proposed. The system output voltage at the next sampling time can be dynamically predicted without complex calculations. As a result, the calculation process for the optimal switching operation of the rectifier can be greatly simplified with good accuracy.
2) A dynamic MPC scheme based on the design of rolling calculation and the dynamic mathematical model is built to achieve an excellent dynamic performance of the IPT system. Besides, the cost function of the MPC scheme is set up to shorten the settling time and to reduce the difference of the control variable of two consecutive control cycles. Thus, the transient process will be substantially shortened without obvious overshoot and power oscillations.
3) To achieve MEET, the P&O method is applied to regulate the phase angle of the inverter to minimize the system input power. Meanwhile, the phase angle of the rectifier is controlled by the MPC scheme to obtain a constant voltage output. Besides, co-operative control principle of MPC and P&O is also provided to avoid the possible unstable phenomenon. Simulation and experiment results validate

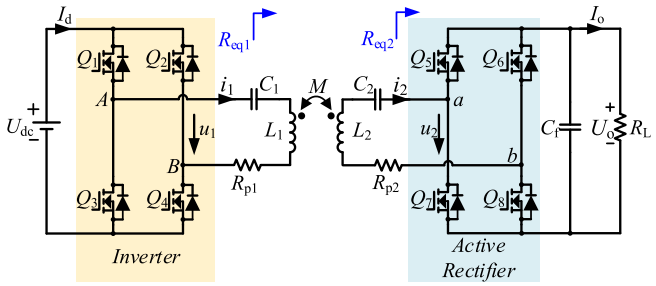


Fig. 1. Schematic diagram of the SS compensated IPT system.

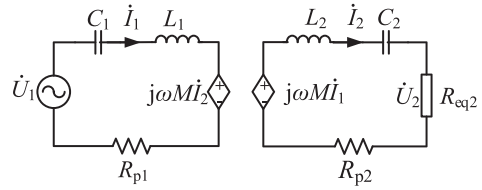

Fig. 2. Mutual inductance circuit model of the SS compensated IPT system.

that MEET can be actually achieved with the P&O scheme, while the dynamic performance is dramatically improved by cooperation with the MPC scheme.

## II. Dynamic Mathematical Model of SS-Compensated IPT Systems

### A. Circuit Modeling

The schematic diagram of the SS-compensated IPT system is shown in Fig. 1. $U_{\rm dc}$ is the system input dc voltage at the primary side. $U_o$ is the output dc voltage at the secondary side. $L_1$ and $L_2$ are the self-inductances of the primary and secondary coils of the magnetic coupler, and their equivalent parasitic resistances are $R_{\rm p1}$ and $R_{\rm p2}$, respectively. $M$ is the mutual inductance between the coupled coils. $C_1$ and $C_2$ denote the series-resonant capacitors, and $C_{\rm f}$ is the filtering capacitor on the dc output side of the rectifier. The system operating frequency is $f_s$, while the angular frequency is $\omega = 2\pi f_s$. $R_{\rm L}$ is the load resistance. Meanwhile, $R_{\rm eq1}$ is the equivalent impedance on the ac output side of the inverter; $R_{\rm eq2}$ is the equivalent impedance on the ac input side of the rectifier.

Schematic diagram in Fig. 1 can be simplified to the mutual inductance circuit model in Fig. 2. The root-mean-square (rms) value of $u_1$ is $U_1$; the rms value of $i_1$ is $I_1$. Similarly, the rms value of $u_1$ and $i_1$ are $U_2$ and $I_2$, respectively.

The Kirchhoff voltage equations can be established as

$$\begin{cases} \dot{U}_1 = (R_{\rm p1} + {\rm j}\omega L_1 + \frac{1}{{\rm j}\omega C_1})\dot{I}_1 + {\rm j}\omega M\dot{I}_2 \\ 0 = {\rm j}\omega M\dot{I}_1 + (R_{\rm p2} + {\rm j}\omega L_2 + \frac{1}{{\rm j}\omega C_2} + R_{\rm eq2})\dot{I}_2. \end{cases} \tag{1}$$

To achieve circuit resonance and unit power factor in the SS-compensated IPT system, resonant frequencies of the primary side and the secondary should be aligned to the operation frequency, i.e., $\omega = 1/\sqrt{L_1C_1} = 1/\sqrt{L_2C_2}$. Thus, currents in the primary coil and the secondary coil could be solved as

$$\begin{cases} \dot{I}_1 = \frac{\dot{U}_1(R_{\rm p2}+R_{\rm eq2})}{\omega^2M^2+R_{\rm p1}(R_{\rm p2}+R_{\rm eq2})} \\ \dot{I}_2 = \frac{-{\rm j}\omega M\dot{U}_1}{\omega^2M^2+R_{\rm p1}(R_{\rm p2}+R_{\rm eq2})}. \end{cases} \tag{2}$$

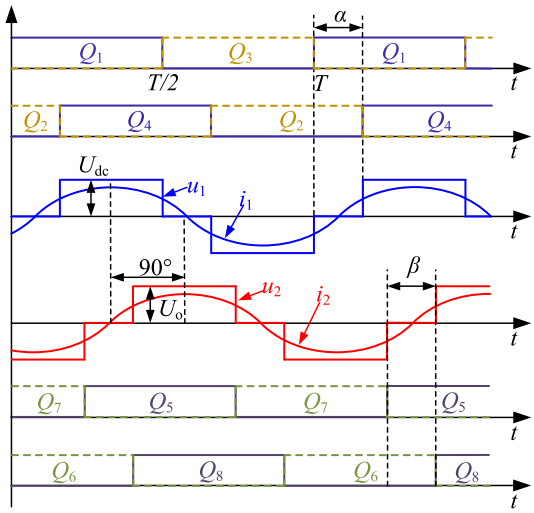

Fig. 3. Waveforms of the switching signals and $u_1$, $u_2$, $i_1$, $i_2$.

According to (2), there is a 90° phase difference between $i_1$ and $i_2$ when the circuit resonates. The waveforms of the switching signals for the inverter and the rectifier, together with $i_1$, $i_2$, $u_1$, and $u_2$, are shown in Fig. 3. While the PSM method is applied on both the inverter and the rectifier, due to the band-pass filtering characteristic of resonant compensations circuits, the fundamental harmonic approximation can be employed to obtain the rms value of $U_1$ and $U_2$. Thus, the following expression can be obtained:

$$\begin{cases} U_1 = \frac{2\sqrt{\cos(\alpha)+1}}{\pi}U_{\rm dc} \\ U_2 = \frac{2\sqrt{\cos(\beta)+1}}{\pi}U_{\rm dc} \end{cases} \tag{3}$$

where $\alpha$ and $\beta$ are the phase shift angles of the inverter and the rectifier, respectively. Moreover, $R_{\rm eq2}$ can be generally expressed as

$$R_{\rm eq2} = \frac{U_2}{I_2} = \left(\frac{4(\cos(\beta)+1)}{\pi^2}\right)R_L. \tag{4}$$

### B. Dynamic Modeling and Analysis

For this SS-compensated IPT system adopting an active rectifier, a dynamic model can be set up based on the rectifier to control the system output voltage. When $\beta = 0°$, the current of $C_f$ can be expressed as

$$C_f\frac{{\rm d}U_o}{{\rm d}t} = -{\rm sgn}(i_2)\cdot i_2 - I_o \tag{5}$$

where

$$i_2 = \sqrt{2}I_2\cdot\cos(\omega t). \tag{6}$$

Substituting (6) into (5) yields

$$C_f \frac{\mathrm{d}U_o}{\mathrm{d}t} = -\sqrt{2}\mathrm{sgn}(\cos(\omega t))I_2 \cos(\omega t) - I_o. \quad (7)$$

After averaging and discretization, (7) can be derived as

$$C_f \frac{\mathrm{d}U_o}{\mathrm{d}t} = I_2 \cdot \frac{2\sqrt{2}}{\pi} - I_o \quad (8)$$

$$C_f \frac{\Delta U_o}{T_P} = I_2(k) \cdot \frac{2\sqrt{2}}{\pi} - I_o(k) \quad (9)$$

where $T_p$ is the control period of the rectifier, and $k$ indicates the sampling instant. According to (9), the dynamic model of the output voltage is given as

$$\Delta U_o(k) = U_o(k+1) - U_o(\mathrm{k}) = \frac{T_P}{C_f}\left[I_2(k)\frac{2\sqrt{2}}{\pi} - I_o(k)\right]. \quad (10)$$

This model uses the amplitude of resonant current $I_2$, dc voltage $U_o$ and current $I_o$ as state variables, which are easy to sample.

If $\beta \neq 0°$, (10) can be derived as

$$U_o(k+1) = \left[\frac{T_P}{C_f}(I_2(k) \cdot \frac{2\sqrt{\cos(\beta(\mathrm{k}))+1}}{\pi} - I_o(k))\right] + U_o(k). \quad (11)$$

According to (10) and (11), it is obvious that controlling the phase shift angle $\beta$ of the rectifier can regulate not only the system output voltage $U_o$, but also $\Delta U_o$, the increment of the system output voltage.

## III. Output Voltage Regulation by the MPC

### A. Brief Introduction of MPC

To mitigate the dynamic drawback caused by load and voltage variations in the SS-compensated IPT system, the MPC scheme is adopted in this article. The MPC scheme is to predict the system future behaviors based on a predictive model and the possible control sets. Then, the optimal control operation is determined in the rolling calculation to minimize the deviation of the control objectives from their references [29]. MPC presents several advantages. In theory, for instance, it can be used in a variety of processes, simple to apply in multivariable systems, and presents a fast dynamic response. Furthermore, it allows for nonlinearities and constraints to be incorporated into the control law in a straightforward manner and it can incorporate nested control loops in only one loop [29], [30].

### B. MPC-Based Controller Design

The principle of the proposed MPC control scheme is shown in Fig. 4. For SS-compensated IPT systems, the MPC scheme can be used to control the phase shift angle $\beta$ of the rectifier so that the system output voltage $U_o$ can be as close as possible to the reference voltage $U_{\mathrm{set}}$. If the number of times of rolling calculation is $N$, ($N$ is the number of the predicted states), the system control variation $m(i)$ can be defined, where $i$ is the order

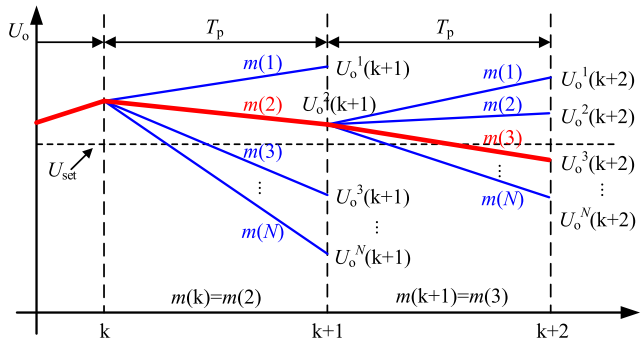


Fig. 4. Principle of the MPC scheme for the IPT system.

of current scroll optimizations ($i = 1, 2, \ldots, N$), and $\cos(\beta^{\mathrm{i}}(k+1)) = \cos(\beta(k)) + m(\mathrm{i})$. The control variation $m(i)$ is the change amount of the cosine value of $\beta$.

By using the predictive model $f$, the system output voltage $U_o(k+1)$ can be predicted as

$$U_o^i(k+1) = f\{U_o(k), I_o(k), I_2(k), \cos(\beta(k)), m(i)\}. \quad (12)$$

Based on the predicted behaviors and the rolling calculation, the value of the control variable $m(k)$ at time $kT_p$ can be determined to minimize the deviation of $U_o(k+1)$ from $U_{\mathrm{set}}$ and the deviation of $\cos(\beta(k))$ from $\cos(\beta(k-1))$.

According to (11), the nonlinear predictive model can be established as (13)

$$U_o{}^i(k+1) = \frac{T_P}{C_f}\left[I_2(k)\frac{2\sqrt{(\cos(\beta(k))+m(i)+1)}}{\pi} - I_o(k)\right] + U_o(k). \quad (13)$$

The corresponding objective function $J$ of the rolling calculation can be formulated as

$$\min J(m(i), U_o(k))$$

$$J(m(i), U_o(k)) = a_1 \sum_{p=1}^{N_P} \left|U_o{}^i(k+1) - U_{\mathrm{set}}\right|^2 + a_2 \sum_{p=1}^{N_p} |m(i)|^2 \quad (14)$$

where $a_1$ and $a_2$ are the weights of the corresponding term values, which are normalized. If there is an $m(i)$ that results in the minimum of $J$, this $m(i)$ should be adapted as $m(k)$, which determined the change in $\cos(\beta)$ at sampling time $kT_p$.

### C. Flowchart of the MPC Controller

The flowchart of the MPC controller for dynamically controlling the SS-compensated IPT system using the MPC strategy can be shown in Fig. 5 and is described as follows.

1) Measure the rms values at sampling time $kT_p$ of the input ac of the rectifier $I_2(k)$, the output dc voltage of the rectifier $U_o(k)$, and the output dc of the rectifier $I_o(k)$.
2) Initialize the control variation $m(i)$ ($i = 1$), and calculate the predicted output voltage $U_o{}^i(k+1)$ according to (13). Then, calculate the cost function $J(i)$ by (14).

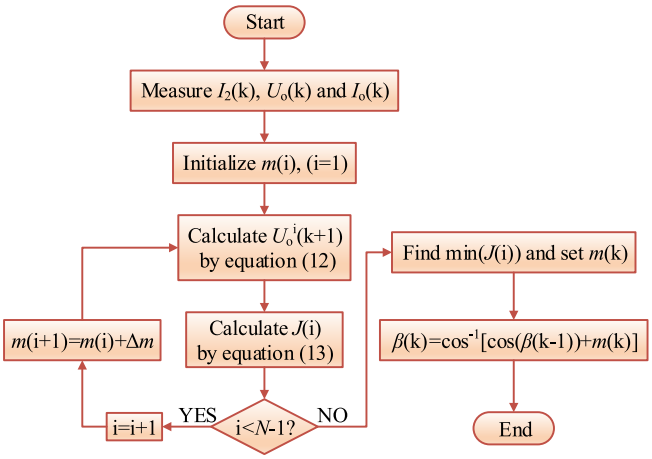


Fig. 5. Flowchart of the MPC scheme with PSM in the IPT system.

3) Determine whether the number of times of rolling calculation $i$ reaches the preset number $n$, and if so, find the minimum value of $J(i)$ by bubble sort method. If not, then $i = i + 1$, returning to step (2).
4) According to the minimum value of $J(i)$ that is found in step (3), the control variation $m(k)$ is determined, and the phase shift angle $\beta$ of the rectifier at time $k$ is determined.

## IV. MEET by the P&O Method

In the previous section, the MPC controller was used to dynamically regulate the phase shift angle of the rectifier. But regulating the phase shift angle of the rectifier will change the equivalent load of each part of the system and affect the energy transfer efficiency as well. Thus, upon the MPC of the rectifier for the phase shift angle regulation, proper control methods are also necessary to control the inverter to achieve MEET.

### A. Analysis of the Overall Efficiency and Power Losses

To achieve MEET in the IPT system, a complete analysis of the overall efficiency and power losses is necessary. Generally, power losses of IPT systems can generally be divided into two parts, one is the power loss in coils and the other is the converter loss. The system efficiency of the SS-compensated IPT system can be derived as

$$\eta = \frac{P_{\text{out}}}{P_{\text{in}}} = \frac{P_{\text{out}}}{P_{\text{out}} + P_{\text{converter\_loss}} + P_{\text{coil\_loss}}} \tag{15}$$

where $P_{\text{in}}$ and $P_{\text{out}}$ are the system input and output power, respectively. $P_{\text{coil\_loss}}$ is the power loss in the coils, and $P_{\text{converter\_loss}}$ is the converter loss.

Substituting (3) into (2), amplitudes of $I_1$ and $I_2$ are given as

$$I_1 = \frac{1}{\omega^2 M^2 + R_{\text{p1}} R_{\text{p2}}} \left( \frac{2\sqrt{\cos(\beta)+1}}{\pi} \omega M \cdot U_{\text{o}} + \frac{2\sqrt{\cos(\alpha)+1}}{\pi} R_{\text{p2}} U_{\text{dc}} \right) \tag{16}$$

and

$$I_2 = \frac{1}{\omega^2 M^2 + R_{\text{p1}} R_{\text{p2}}} \left( \frac{2\sqrt{\cos(\alpha)+1}}{\pi} \omega M \cdot U_{\text{dc}} - \frac{2\sqrt{\cos(\beta)+1}}{\pi} R_{\text{p1}} U_{\text{o}} \right). \tag{17}$$

Since the values of the parasitic resistances $R_{\text{p1}}$ and $R_{\text{p2}}$ can be ignored, (16) and (17) can be simplified as

$$I_1 = \frac{2 \cdot \sqrt{\cos(\beta)+1} \cdot U_{\int \text{o}}}{\pi \cdot \omega \cdot M} \tag{18}$$

and

$$I_2 = \frac{2 \cdot \sqrt{\cos(\alpha)+1} \cdot U_{\text{dc}}}{\pi \cdot \omega \cdot M}. \tag{19}$$

To regulate the output voltage to the desired value, the phase shift angle of the rectifier should meet

$$\cos(\beta) = \left( \frac{\pi U_o}{2 I_2 R_{\text{L}}} \right)^2 - 1. \tag{20}$$

Substitute (20) into (18) and (19), the current in the primary coil $I_1$ and the phase shift angle of the rectifier $\beta$ can be solved

$$I_1 = \frac{\pi U_o^2}{2 R_L U_{\text{dc}} \sqrt{\cos(\alpha)+1}} \tag{21}$$

$$\beta = 2 \arccos \left( \frac{\pi^2 \omega U_o M}{8 R_L U_{\text{dc}} \cos\left(\alpha/2\right)} \right). \tag{22}$$

Thus, coil loss in this IPT system can be expressed as

$$\begin{aligned} P_{\text{coil\_loss}} &= I_1^2 R_{\text{p1}} + I_2^2 R_{\text{p2}} \\ &= \frac{\pi^2 U_o^4}{4 R_{\text{L}}^2 U_{\text{dc}}^2 (\cos(\alpha)+1)} R_{\text{p1}} + \frac{4(\cos(\alpha)+1) U_{\text{dc}}^2}{\pi^2 \omega^2 M^2} R_{\text{p2}}. \end{aligned} \tag{23}$$

On the other hand, the converter loss can be divided into conducting loss and switching loss, while ignoring the dead time of the converter signals, these two parts of power losses of the inverter and the rectifier can be expressed as [40]

$$\begin{cases} P_{c1} = 2 R_{DS} I_1^2 + \frac{\sqrt{2} U_{SD} I_1}{\pi} \left[ 2 - 2\cos\left(\frac{\alpha}{2}\right) \right] \\ P_{c2} = 2 r_{SD} I_2^2 + \frac{\sqrt{2} U_{SD} I_2}{\pi} \left[ 2 - 2\cos\left(\frac{\beta}{2}\right) \right] \\ P_{\text{s1}} = 2\sqrt{2} U_{\text{dc}} I_1 \sin\left(\frac{\alpha}{2}\right) \left( \frac{E_{\text{on}} + E_{\text{off}}}{U_{DD} I_D} + \frac{Q_{RR}}{I_{R\_D}} \right) f_{\text{s}} \\ P_{\text{s2}} = 2\sqrt{2} U_{\text{o}} I_2 \sin\left(\frac{\beta}{2}\right) \left( \frac{E_{\text{on}} + E_{\text{off}}}{U_{DD} I_D} + \frac{Q_{\text{RR}}}{I_{R\_D}} \right) f_{\text{s}} \end{cases} \tag{24}$$

where $P_{\text{c1}}$ and $P_{\text{c2}}$ are the conducting losses of the inverter and rectifier, respectively, and $P_{\text{s1}}$ and $P_{\text{s2}}$ are the switching losses. $R_{DS}$, $U_{SD}$, $r_{SD}$, $E_{\text{off}}$, $Q_{RR}$, $U_{DD}$, $I_D$, and $I_{R\cdot D}$ are some inherit parameters of the MOSFET in the inverter and the rectifier, which can be found or fitted in the datasheet of the MOSFET. Substituting

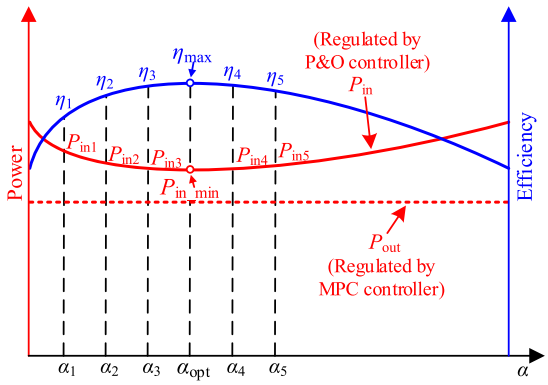


Fig. 6. Graphical illustration of the P&O control scheme in the IPT system.

(19), (21), and (22) into (24), one can be derived as

$$\begin{cases} P_{c1} = \dfrac{U_o^2\left(\pi^2 R_{DS} U_o^2 + 4R_L U_{SD} U_{dc}\cdot\cos\left(\frac{\alpha}{2}\right)\left(1-\cos\left(\frac{\alpha}{2}\right)\right)\right)}{4R_L^2 U_{dc}^2\cdot\cos^2\left(\frac{\alpha}{2}\right)} \\ P_{c2} = \dfrac{8R_L U_{SD} U_{dc}\omega M\cos\left(\frac{\alpha}{2}\right) - \pi^2 U_o U_{SD}\omega^2 M^2 + 16R_L r_{SD} U_{dc}^2\cos^2\left(\frac{\alpha}{2}\right)}{\pi^2 R_L \omega^2 M^2} \\ P_{s1} = \dfrac{2\pi f_s U_o^2}{R_L} tan\left(\frac{\alpha}{2}\right)\left(\dfrac{E_{on}+E_{off}}{U_{DD} I_D} + \dfrac{Q_{RR}}{I_{R\_D}}\right) \\ P_{s2} = \dfrac{2 f_s U_o U_{dc}}{\pi\omega M}\cos\left(\frac{\alpha}{2}\right)\left(\dfrac{E_{on}+E_{off}}{U_{DD} I_D} + \dfrac{Q_{RR}}{I_{R\_D}}\right) \\ \quad \times\sqrt{64 - \dfrac{\pi^4\omega^2 M^2 U_o^2}{R_L^2 U_{dc}^2\cdot\cos^2\left(\frac{\alpha}{2}\right)}}. \end{cases} \tag{25}$$

As a result, the converter losses in the IPT system can be expressed as

$$P_{converter\_loss} = P_{c1} + P_{c2} + P_{s1} + P_{s2}. \tag{26}$$

### B. Design of the P&O Controller for Efficiency Improving

Actually, according to (23) and (25), it is hard to express the complete and exact expression of the overall power loss. Moreover, with such complicated nonlinear trigonometric function calculations, it is also difficult to solve the optimal $\alpha$ to minimize the overall power loss. However, to achieve MEET in the IPT system, a simple but available method minimizes the input power under the premise that the out voltage and power are ensured. For this purpose, the P&O method based phase shift control is adopted for minimizing the system dc input current $I_d$, and the system maximum overall efficiency can be searched by regulating the inverter phase shift angle $\alpha$, as shown in Fig. 6.

The inverter phase shift angle $\alpha$ is perturbed by the proposed P&O controller, and the input power $P_{in}$ under different $\alpha$ is compared to determine the searching direction for MEET. To make sure whether the system has tracked the maximum efficiency point or not, the system dc input current $I_d$ and the output voltage $U_o$ are fed back into the P&O controller. The maximum efficiency point will be achieved by minimizing $I_d$, which indicates the minimum $P_{in}$, while $U_o$ is guaranteed priority by the MPC controller. If $U_o$ is lower than the reference value, $\alpha$ should be decreased immediately.

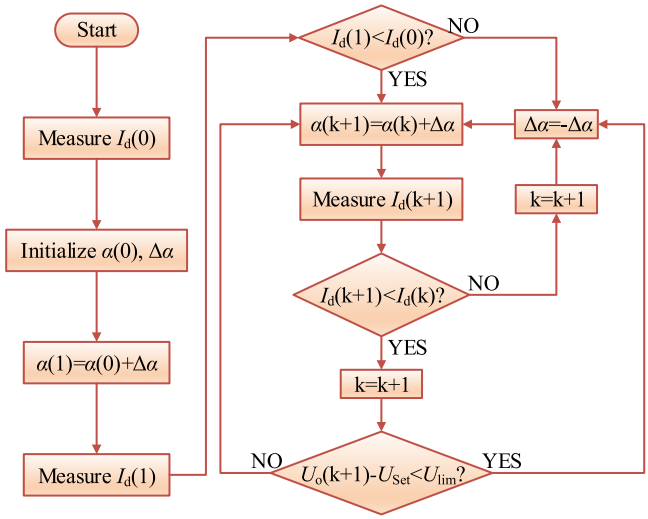


Fig. 7. Flowchart of the P&O scheme with PSM in the IPT system.

### C. Flowchart of the P&O Controller

The P&O-based PSM scheme used in the inverter for achieving MEET can be shown in Fig. 7 and is described as follows.

1) Apply the initial phase shift angle $\alpha(0)$ and the change amount $\Delta\alpha$ to the inverter and measure the system input current $I_d(0)$, where $\alpha(1) = \alpha(0) + \Delta\alpha$.
2) At the next sampling period, the phase shift angle $\alpha$ is increased by an increment angle $\Delta\alpha$ to obtain the phase shift angle $\alpha(1)$ of the inverter during the period and measure the current $I_d(1)$.
3) The direction of the perturbation observation ($\Delta\alpha$ is positive or negative) is determined by comparing $I_d(0)$ and $I_d(1)$. If $I_d(1) < I_d(0)$, it means that the system efficiency is actually increased, and $\alpha$ is becoming close to the optimal phase angle $\alpha_{opt}$. Then, $\alpha$ should be continuously increased by $\alpha(k+1) = \alpha(k) + \Delta\alpha$. Here, $k$ represents the sampling time $kT_r$. If $I_d(1) > I_d(0)$, it means that the increase of $\alpha$ deviates from $\alpha_{opt}$, or the system efficiency should be decreased by $\Delta\alpha$. Then, $\alpha$ is reduced by $\alpha(k+1) = \alpha(k) + \Delta\alpha$, where $\Delta\alpha$ has been converted to $-\Delta\alpha$.
4) For the two directions of perturbation observation, the output voltage $U_o$ and the current in the secondary coil $I_d$ at the sampling time $k+1$ are compared with the voltage and the current at the previous sampling time $k$. If $I_d(k+1) < I_d(k)$ and $|U_o(k) - U_{set}| < U_{lim}$, it means that the system efficiency is increased and the output voltage $U_o$ still satisfies the system requirement. Thus, increasing $\alpha$ or decreasing $\alpha$ should be continued to further improve the system efficiency. If $I_d(k+1) > I_d(k)$ or $|U_o(k) - U_{set}| > U_{lim}$, it indicates that the change of $\alpha$ cannot further reduce the system input current $I_d$ or the output voltage $U_o$ does not satisfy the system requirement. Then, $\Delta\alpha$ should be converted to $-\Delta\alpha$.

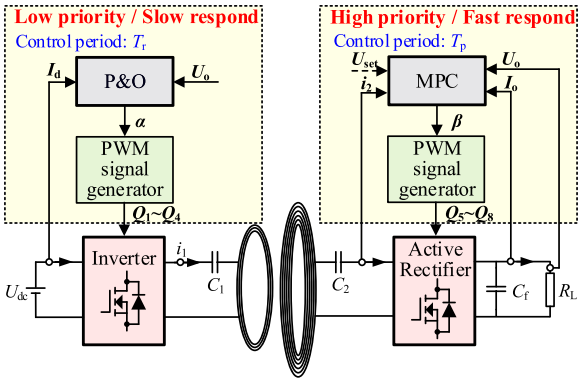


Fig. 8. Block diagram of the proposed control scheme for the IPT system.

### D. Cooperative Control Principle of MPC and P&O

Due to the time delay caused by sampling circuit, communication, and MCU calculation, instability issues or unacceptable inaccurate results may occur in many power electronic systems, especially in systems that contain two or more controllers [41]–[43]. In the proposed IPT system, the variation of the current in the secondary coil $I_2$ depends on and lags behind the regulation of the phase shift angle $\alpha$. Meanwhile, the variation of the current in the primary coil $I_1$ and the dc input current $I_{\rm d}$ also depend on and lags behind the regulation of the phase shift angle $\beta$. Thus, if $\alpha$ and $\beta$ are regulated at the same moment, oscillation or instability of the system may occur due to the delay in current variation.

Here, two aspects should be considered. First, due to the possible oscillation or instability of the system, regulation of the inverter phase shift angle $\alpha$ and the rectifier phase shift angle $\beta$ at the same moment should be avoided. Second, the phase shift angle $\beta$ should be regulated rapidly to handle the dynamic variations from the load and the system input. To address the first issue, the phase shift angle $\alpha$ should not follow the variation of $\beta$ by the same control period $T_p$. Then, to address the second issue, since MPC features a fast dynamic response, it can be applied to deal with the variations from system power source and loads. In the specific operation, the MPC controller should be used to make the output voltage constant as the priority target, and $\alpha$ is slowly regulated with $T_r$ ($T_r << T_p$) as the control period of the inverter to achieve dynamic MEET by the P&O controller.

## V. Simulation Results

### A. System and Parameters Design

The whole control block diagram of the IPT system is shown in Fig. 8, the MPC controller and the P&O controller are adapted for constant output voltage and maximum system efficiency, respectively. Afterload or input voltage varied, the stability of the output voltage $U_o$ and the output power $P_{\rm out}$ should be prioritized by the MPC controller. Then, the P&O controller can tune the inverter phase shift angle $\alpha$ for minimizing the system input power $P_{\rm in}$ so that the maximum efficiency point can be tracked.

TABLE I
Main Parameters of the IPT System.

| Symbol | Parameter | Value | Unit |
|---|---|---|---|
| $L_1$ | Coil inductance of the transmitter | 184.66 | $\mu$H |
| $L_2$ | Coil inductance of the receiver | 568.27 | $\mu$H |
| $R_{\rm p1}$ | Equivalent resistances of | 0.21 | Ω |
| $R_{\rm p2}$ | Coil resistance of the receiver | 0.71 | Ω |
| $C_1$ | Resonant capacitance of $L_1$ | 21.96 | nF |
| $C_2$ | Resonant capacitance of $L_2$ | 6.96 | nF |
| $M$ | Mutual inductance between the transmitter and receiver | 64.20 | $\mu$H |
| $C_{\rm f}$ | Filtering capacitance of the rectifier | 940 | $\mu$F |
| $f_{\rm s}$ | System operating frequency | 80 | kHz |

TABLE II
Control Parameters of the MPC Controller and PI Controller

| Symbol | Parameter | Value | Unit |
|---|---|---|---|
| $T_{\rm p}$ | Control period of the rectifier | 500 | $\mu$s |
| $U_{\rm set}$ | Setting value of the output voltage | 100 | V |
| $K_{\rm p}$ | The proportional tuning coefficient | 0.3217 | |
| $K_{\rm i}$ | The integral tuning coefficient | 0.8848 | |
| $N_{\rm p}$ | Prediction horizon | 1 | |
| $a_1$ | The weight of the output voltage deviation | 0.9 | |
| $a_2$ | The weight of the increment of cos($\beta$) | 0.1 | |
| $N$ | The number of times of rolling calculation | 11 | |

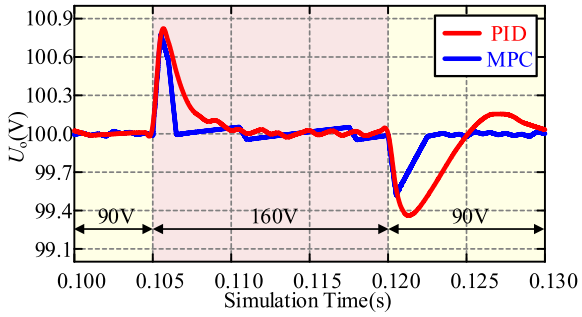


Fig. 9. Comparisons of $U_o$ between the MPC controller and the PI controller when $U_{\rm dc}$ changed.

The software platform SIMULINK is used for simulation research, and the system input voltage $U_{\rm dc}$ and the system load resistance $R_{\rm L}$ are dynamically regulated to compare the dynamic performance of the IPT system under the discrete PI control and the MPC control. Table I lists the main circuit system parameters. Parameters of the discrete PI controller and the MPC controller are shown in Table II.

### B. Dynamic Response Comparison Between MPC and PID

Comparisons of $U_o$ between the MPC controller and the PI controller, when $U_{\rm dc}$ changed and $R_L$ changed, are shown in Figs. 9 and 10.

In the first test, the input dc voltage $U_{\rm dc}$ steps from 90 to 160 V at 0.105 s, and backs to 90 V at 0.120 s. When $U_{\rm dc}$ steps, the system can still return to the steady state in a short time, as presented in Fig. 9. The average time to return the steady state is

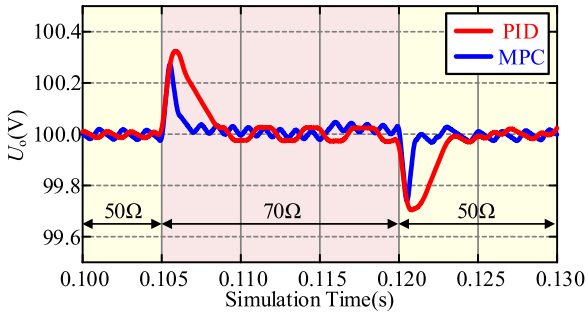


Fig. 10. Comparisons of $U_o$ between the MPC controller and the PI controller when $R_L$ changed.

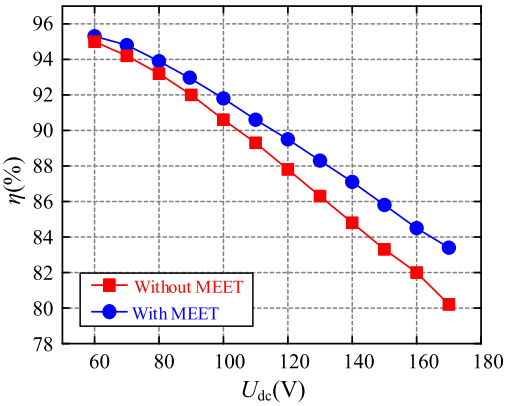


Fig. 11. Comparisons of $\eta$ in the simulation between the system with MEET and without MEET.

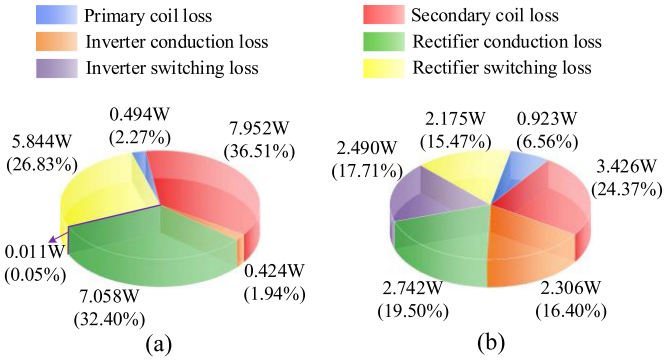


Fig. 12. Simulated power loss distributions when $U_{\rm dc} = 120$ V and $R_L = 70\ \Omega$ (a) without MEET and (b) with MEET.

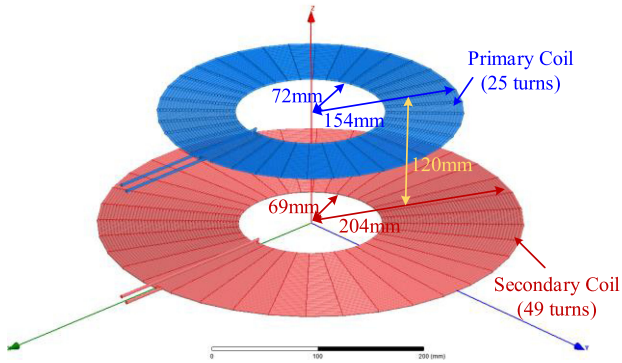


Fig. 13. Schematic diagram and parameters of the coupled coils.

about 1.67 ms with the MPC controller, while the system costs are at least twice as long to return the steady state by using the PI controller.

In the second test, the system load $R_{\rm L}$ steps from 50 to 70 Ω at 0.105 s, and backs to 50 Ω at 0.120 s. The waveforms of $U_o$ under such load variation are shown in Fig. 10. With the MPC controller, when $R_L$ steps, the system returns to the steady state in about 1.22 ms on average. Similarly, the PI controller needs twice settling time for returning $U_o$ to the steady state.

### C. Overall Efficiency and Power Loss Comparison

Meanwhile, the system efficiency $\eta$ can be improved by the P&O controller. Setting the system load $R_{\rm L}$ to 70 Ω, and $U_{\rm dc}$ is increased from 60 to 170 V to test the effect of the P&O method under different $U_{\rm dc}$. In the simulation, after a searching process for the minimum system input current, the phase shift angle of the inverter and the rectifier can be obtained by using SIMULINK. Moreover, to achieve an accurate analysis of power losses in the IPT system, including converter losses and coil losses, LTspice software is applied to compare the overall efficiency $\eta$ of the system with or without MEET. The simulation results are shown in Fig. 11. When $U_{\rm dc} = 120$ V and $R_L = 70\ \Omega$, simulated power loss distributions of the IPT system with and without MEET are shown in Fig. 12.

## VI. Experimental Verification

### A. Prototype Setup

In order to verify the feasibility of the proposed controllers, the experimental setup of a SS-compensated IPT system is built. The system consists of a dc voltage source, a high-frequency inverter, a pair of coupled coils and their resonance compensation networks, a rectifier, a load, and controllers with sensors. The structure and relevant parameters of the coils are shown in Fig. 13. The controller uses low-cost MCU STM32F103. A photograph of the complete experimental setup, with parameters in Table I, is shown in Fig. 14.

### B. Dynamic Response Comparison

Under the MPC scheme and the PI control scheme, when the system load resistance $R_L$ steps from 50 to 70 Ω, the waveforms of $U_o$, $u_1$, $i_2$, and $i_1$ are shown in Figs. 15 and 16. As shown in Fig. 15, with the MPC controller, the system output voltage $U_o$ is kept stable when the load resistance $R_L$ steps and the current $i_1$ decreases accordingly with increased load. Meanwhile, no overshoot voltage can be observed.

As shown in Fig. 16, with the PI controller, when the load steps, the system output voltage $U_o$ has a large oscillation. The overshoot voltage is about 23.7 V, and the settling time is about 204 ms, which is much larger than the system with the MPC controller.

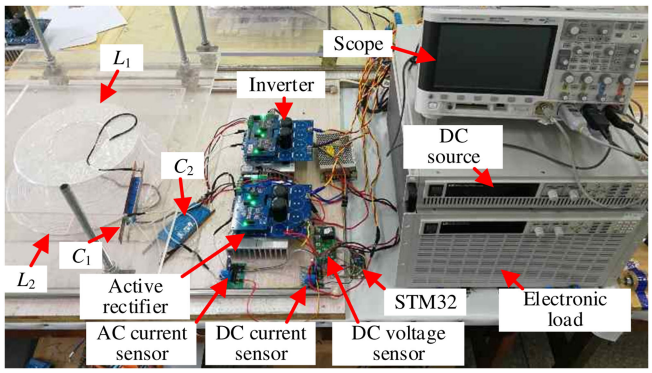


Fig. 14. Photograph of the experiment setup.

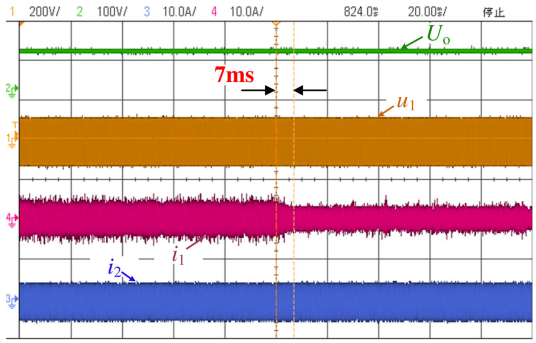


Fig. 15. Waveforms of $U_o$, $u_1$, $i_1$, $i_2$ when $R_L$ is changed from 50 to 70 Ω with the MPC controller.

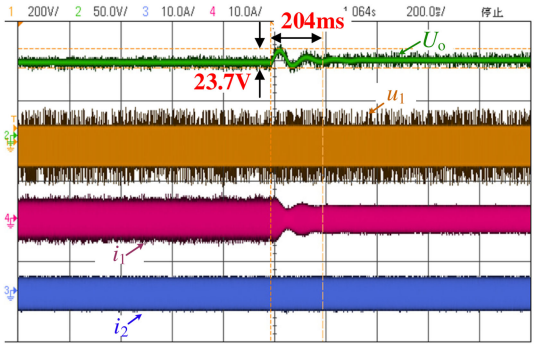


Fig. 16. Waveforms of $U_o$, $u_1$, $i_1$, $i_2$ when $R_L$ is changed from 50 to 70 Ω with the PI controller.

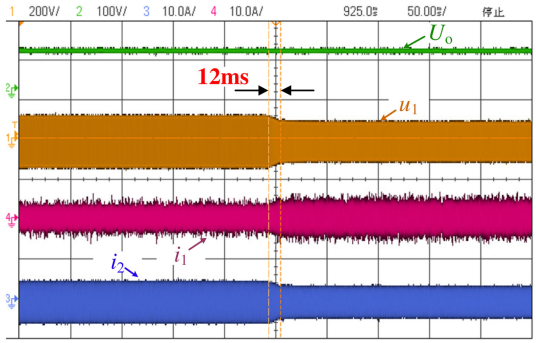


Fig. 17. Waveforms of $U_o$, $u_1$, $i_1$, $i_2$ when $U_{dc}$ is changed from 120 to 90 V with the MPC controller.

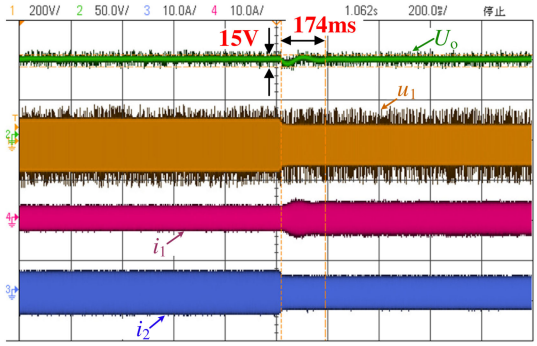


Fig. 18. Waveforms of $U_o$, $u_1$, $i_1$, $i_2$ when $U_{dc}$ is changed from 120 to 90 V with the PI controller.

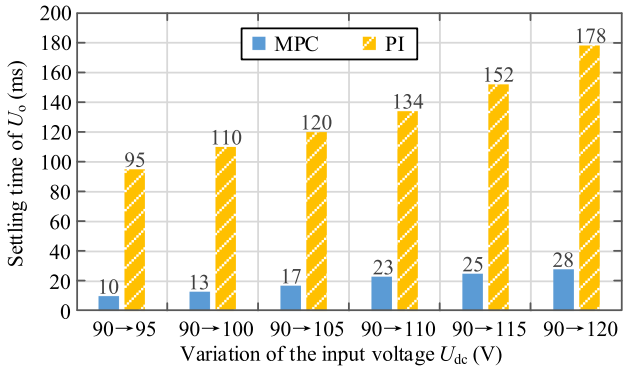


Fig. 19. Comparisons of the settling time of $U_o$ between the MPC controller and the PI controller when $U_{dc}$ steps.

Under the MPC control and the PI control, when the system input voltage $U_{dc}$ steps from 120 to 90 V, the waveform of $U_o$, $u_1$, $i_2$, and $i_1$ are shown in Figs. 17 and 18. As shown in Fig. 17, when the input voltage $U_{dc}$ is changed, the system output voltage $U_o$ presents no significant variation by using the MPC controller, and the inverter input voltage $u_1$ reduced accordingly and smoothly when $U_{dc}$ steps from 120 to 90 V within about 15 ms.

As shown in Fig. 18, under the PI control, when the input voltage steps, the system output voltage $U_o$ has a large overshoot and transient process. The overshoot voltage is about 15 V, and the settling time is about 174 ms, which is much larger than the system under the MPC control.

The experimental results in Figs. 19 and 20 show that the MPC method has better dynamic performance when $U_{dc}$ or $R_L$ changes, compared with the traditional PI control method. The improvement of the settling time is on average about 85.7%. Furthermore, the overshoot is smaller and hard to measure under the MPC control, which significantly improves the dynamic performance of the SS-compensated IPT system.

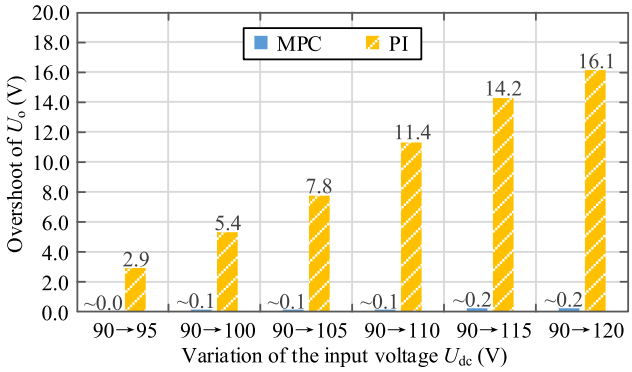


Fig. 20. Comparisons of the overshoot of $U_o$ between the MPC controller and the PI controller when $U_{dc}$ steps.

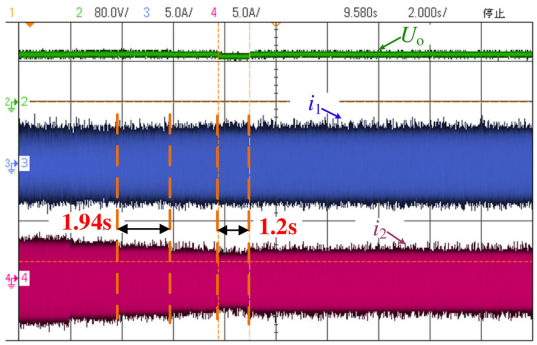


Fig. 21. Waveforms of $U_o$, $i_1$, $i_2$ in search process of P&O.

### C. Efficiency Improving Results of MEET

Subsequently, another test is taken to further validate the MEET by using the proposed control method. The load resistance $R_L$ is set to 50 Ω. The input voltage $U_{dc}$ is 120 V. The phase shift angle $\beta$ of the rectifier is regulated by the MPC controller, and the phase shift angle $\alpha$ of the inverter is regulated by the P&O controller to improve the output efficiency.

The waveforms of $U_o$, $i_1$, and $i_2$ during the process of the P&O scheme are shown in Fig. 21. As shown in Fig. 21, when the system input voltage $U_{dc}$ and the load resistance $R_L$ are fixed, regulating the phase shift angle of the inverter $\alpha$ by the P&O controller can effectively reduce the system input current $I_d$ and the current in the secondary coil $i_2$. In the process of reducing $i_2$, the phase shift angle $\beta$ of the rectifier with the MPC controller is also reduced. Thus, the power loss in the secondary coil can be obviously reduced and the energy transfer efficiency of the system is actually improved. After a searching process for the optimal efficiency point, the MEET effect can be achieved. In some specific operations, when the system output voltage $U_o$ continues to be less than the system set value for a while, the inverter phase shift angle $\alpha$ will be automatically reduced to ensure the requirements of the output voltage and output power.

After verifying the feasibility and effectiveness of the algorithm, the load resistance $R_L$ is set to 50 Ω, and the energy transmission efficiency $\eta$ is measured when the system is controlled by P&O method under different input voltages $U_{dc}$.

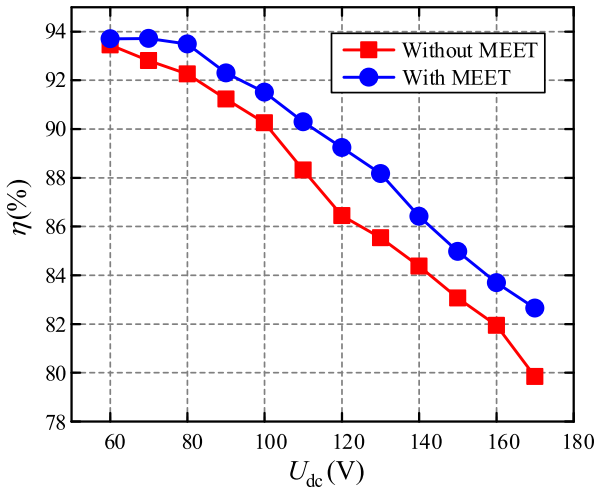


Fig. 22. Comparisons of $\eta$ in the experiment between the system with MEET and without MEET.

It can be seen from Fig. 22 that the larger the input voltage $U_{dc}$ is, the lower the system energy transmission efficiency $\eta$ will be. And as expected, system efficiency is significantly improved when the system is controlled by the P&O method to track the maximum efficiency point of the system. The experiment results show that the maximum improvement is over 3%.

### D. Comparison to Previous Methods With MEET

The idea for achieving MEET in IPT systems has been published in some papers [21], [44]–[47]. However, it should emphasize that the main objectives and contributions of this article are to optimize the system overall efficiency with an excellent dynamic response by using the MPC controller. Therefore, the main focus of this article is quite different from previous works. In order to clarify the novelty of this article, the comparisons with the state-of-the-art are discussed below.

In [44] and [45], a method by regulating the duty cycle of the dc–dc converter including BUCK and BOOST converter is proposed to maintain the output voltage while improving the system efficiency by P&O [44] and linear control scheme [45]. This method does improve the overall efficiency of the IPT system. However, these two dc–dc converters will bring extra power loss, which limits the further improvement of the system efficiency. Besides, the overshoot and the settling time of the output voltage still need to be improved.

In [46], a method by regulating the phase-shift of the active rectifier to adjust the load impedance is proposed to improve the system efficiency, while a dc–dc converter is applied to provide a controllable output control. However, this proposed method cannot maintain a high efficiency with various coupling coefficient and loads. Besides, the dynamic response of the output voltage is missing in [46]. In [21], the active rectifier is used to regulate the resistance and reactance of the load to improve the efficiency, while the inverter is regulated for a constant output voltage. However, the mutual inductance should be fixed and need a measurement for improving the efficiency. Moreover, according

TABLE III
SUMMARY AND COMPARISON OF THE PREVIOUS MEET METHODS

| References | Operating frequency | Air gap | Coupling coefficient | Maximum efficiency | Maximum settling time | Overshoot |
|---|---|---|---|---|---|---|
| [44] | 515kHz | 3~27cm | 0.03~0.61 | 88% | | |
| [45] | 200kHz | 2.5cm, 3.3cm, 4.5cm | 0.1217, 0.1739, 0.2541 | 90% | <300ms ($R_L$:55Ω→10Ω) | ~6V ($U_o$:30V, $R_L$:55Ω→10Ω) |
| [46] | 140kHz | 0.3cm, 1cm | 0.3, 0.6 | 83% | | |
| [21] | 30kHz | 10cm | 0.186 | 91.70% | >200ms ($R_L$:30Ω→20Ω) | >40V ($U_o$:120V, $R_L$:30Ω→20Ω) |
| [47] | 85kHz | 15cm | 0.217 | 91.57% | >20ms ($R_L$:200Ω→60Ω) | >15V ($U_o$:100V, $R_L$:200Ω→60Ω) |
| This paper | 80kHz | 12cm | 0.201 | 93.69% | ~8ms ($R_L$:70Ω→50Ω) | ~0.1V ($U_o$:100V, $R_L$:70Ω→50Ω) |

to the waveforms in [21], when load resistance changes, the overshoot and the settling time of the output voltage still need to be taken seriously. In [47], the active rectifier is used to optimize the current-stress of the WPT system. The system efficiency can be improved by reducing the current-stress of the converters. However, this method may not achieve the optimal overall efficiency because the coil loss is not considered. Moreover, the waveforms in [45] show that the settling time of the output voltage is more than 20 ms when load resistance changes, and the overshoot cannot be ignored either.

Compared to the previous methods, the contributions of this article are that a stable output voltage can be ensured when the load resistance, input voltage changes, or the phase shift angle of the inverter changes. The settling time of the output voltage will be sharply shortened with a minor overshoot in the MEET process, while the maximum overall efficiency is actually achieved. Besides, the proposed system is able to obtain a higher overall efficiency compared with the system with dc–dc converter. The key parameters of these mentioned methods above are summarized and listed in Table III.

## VII. CONCLUSION

In this article, the MPC controller is applied to control the dc output voltage of the rectifier of the SS-compensated IPT system. Compared with the traditional PI controller, this control scheme has a better effect in improving the dynamic performance of the IPT system. Experiment results show that when the system input voltage or the load resistance steps, the settling time is shortened by 85.7%, and the overshoot is hardly seen under various conditions. Such improvement of the dynamic performance can effectively protect the load equipment from the potential-high-voltage overshoot with the long settling time. While maintaining the output voltage stability by the MPC controller, using P&O scheme to regulate the phase shift angle of the inverter can effectively improve the system efficiency by 1.85% on average. In future work, a complete IPT system considering more details, including shielding, ZVS operation, parameter estimation, etc., will be built for a practical and reliable dynamic IPT system.

## REFERENCES


[1] F. Lu, H. Zhang, H. Hofmann, and C. Mi, "A double-sided LCLC-compensated capacitive power transfer system for electric vehicle charging," *IEEE Trans. Power Electron.*, vol. 30, no. 11, pp. 6011–6014, Nov. 2015.

[2] B. Nguyen *et al.*, "An efficiency optimization scheme for bidirectional inductive power transfer systems," *IEEE Trans. Power Electron.*, vol. 30, no. 11, pp. 6310–6319, Nov. 2015.

[3] S. Samanta and A. Rathore, "A new inductive power transfer topology using direct AC–AC converter with active source current waveshaping," *IEEE Trans. Power Electron.*, vol. 33, no. 7, pp. 5565–5577, Jul. 2018.

[4] M. Lu and K. Ngo, "Systematic design of coils in series–series inductive power transfer for power transferability and efficiency," *IEEE Trans. Power Electron.*, vol. 33, no. 4, pp. 3333–3345, Apr. 2018.

[5] Y. Li, J. Hu, F. Chen, S. Liu, Z. Yan, and Z. He, "A new-variable-coil-structure-based IPT system with load-independent constant output current or voltage for charging electric bicycles," *IEEE Trans. Power Electron.*, vol. 33, no. 10, pp. 8226–8230, Oct. 2018.

[6] B. Strassner and K. Chang, "A circularly polarized rectifying antenna array for wireless microwave power transmission with over 78% efficiency," in *Proc. IEEE MTT-S Int. Microw. Symp. Dig.*, 2002, pp. 1535–1538.

[7] D. Patil, M. Mcdonough, J. Miller, B. Fahimi, P. T. Balsara, "Wireless power transfer for vehicular applications: overview and challenges," *IEEE Trans. Transp. Electrific.*, vol. 4, no. 1, pp. 3–37, Mar. 2018.

[8] S. Lukic and Z. Pantic, "Cutting the cord: Static and dynamic inductive wireless charging of electric vehicles," *IEEE Electrific. Mag.*, vol. 1, no. 1, pp. 57–64, Sept. 2013.

[9] G. Covic, J. Boys, M. Kissin, and H.G. Lu, "A three-phase inductive power transfer system for roadway-powered vehicles," *IEEE Trans. Ind. Electron.*, vol. 54, no. 6, pp. 3370–3378, Dec. 2007.

[10] Y. Li, J. Hu, T. Lin, X. Li, F. Chen, Z. He, and R. Mai, "A new coil structure and its optimization design with constant output voltage and constant output current for electric vehicle dynamic wireless charging," *IEEE Trans. Ind. Informat.*, vol. 15, no. 9, pp. 5244–5256, Sept. 2019.

[11] Y. Jang, E. Suh, and J. Kim, "System architecture and mathematical models of electric transit bus system utilizing wireless power transfer technology," *IEEE Syst. J.*, vol. 10, no. 2, pp. 495–506, Jun. 2016.

[12] J. Huh, S. Lee, W. Lee, G. Cho, and C. T. Rim, "Narrow-width inductive power transfer system for online electrical vehicles," *IEEE Trans. Power Electron.*, vol. 26, no. 12, pp. 3666–3679, Dec. 2011.

[13] T. Maekawa, Q. Duong, T. Higashino, and M. Okada, "Fast receiver-side load control based on electromagnetic distribution for wireless power transfer using parallel line feeder," in *Proc. IEEE Wireless Power Transfer Conf.*, 2016, pp. 1–4.

[14] W. Shi, J. Deng, Z. Wang, and X. Cheng, "The start-up dynamic analysis and one cycle control-PD control combined strategy for primary-side controlled wireless power transfer system," *IEEE Access*, vol. 6, pp. 14439–14450, Mar. 2018.

[15] Y. Chung, C. Lee, H. Kang, and Y. Park, "Design considerations of superconducting wireless power transfer for electric vehicle at different inserted resonators," *IEEE Trans. Appl. Supercond.*, vol. 26, no. 4, pp. 1–5, Jun. 2016.
[16] K. Hwang, S. Chung, U. Yoon, M. Lee, and S. Ahn, "Thermal analysis for temperature robust wireless power transfer systems," in *Proc. IEEE Wireless Power Transfer*, 2013, pp. 52–55.
[17] H. Li, Y. Liu, K. Zhou, Z. He, W. Li, and R. Mai, "Uniform power IPT system with three-phase transmitter and bipolar receiver for dynamic charging," *IEEE Trans. Power Electron.*, vol. 34, no. 3, pp. 2013–2017, Mar. 2019.
[18] D. Ahn and S. Hong, "Wireless power transmission with self-regulated output voltage for biomedical implant," *IEEE Trans. Ind. Electron.*, vol. 61, no. 5, pp. 2225–2235, May 2014.
[19] R. Mai, P. Yue, Y. Liu, Y. Zhang, and Z. He, "A dynamic tuning method utilizing inductor paralleled with load for inductive power transfer," *IEEE Trans. Power Electron.*, vol. 33, no. 12, pp. 10924–10934, Dec. 2018.
[20] M. Fu, H. Yin, X. Zhu, and C. Ma, "Analysis and tracking of optimal load in wireless power transfer systems," *IEEE Trans. Power Electron.*, vol. 30, no. 7, pp. 3952–3963, Jul. 2015.
[21] R. Mai, Y. Liu, Y. Li, P. Yue, G. Cao, and Z. He, "An active-rectifier-based maximum efficiency tracking method using an additional measurement coil for wireless power transfer," *IEEE Trans. Power Electron.*, vol. 33, no. 1, pp. 716–728, Jan. 2018.
[22] W. Zhong and S. Hui, "Maximum energy efficiency tracking for wireless power transfer systems," *IEEE Trans. Power Electron.*, vol. 30, no. 7, pp. 4025–4034, Dec. 2018.
[23] Y. Nagatsuka, N. Ehara, Y. Kaneko, S. Abe, and T. Yasuda, "Compact contactless power transfer system for electric vehicles," in *Proc. Int. Power Electron. Conf*, 2010, pp. 807–813.
[24] W. Zhang, S. C. Wong, C. K. Tse, and Q. Chen, "Design for efficiency optimization and voltage controllability of series–series compensated inductive power transfer systems," *IEEE Trans. Power Electron.*, vol. 29,no. 1, pp. 191–200, Jan. 2014.
[25] K. Hata, T. Imura, and Y. Hori, "Dynamic wireless power transfer system for electric vehicles to simplify ground facilities - power control and efficiency maximization on the secondary side," in *Proc. IEEE Appl. Power Electron. Conf. Expo.*, 2016, pp. 1731–1736.
[26] L. Xiang, Y. Sun, C. Tang, X. Dai, and C. Jiang, "Design of crossed DD coil for dynamic wireless charging of electric vehicles," in *Proc. IEEE PELS Workshop Emerg. Technol. , Wireless Power Transfer*, 2017, pp. 1–5.
[27] M. Neath, A. Swain, U. Madawala, and D. Thrimawithana, "An optimal PID controller for a bidirectional inductive power transfer system using multiobjective genetic algorithm," *IEEE Trans. Power Electron.*, vol. 29, no. 3, pp. 1523–1531, Mar. 2014.
[28] Y. Yang, W. Zhong, S. Kiratipongvoot, S. Tan, S. Y. R. Hui, "Dynamic improvement of series–series compensated wireless power transfer systems using discrete sliding mode control," *IEEE Trans. Power Electron.*, vol. 33, no. 7, pp. 6351–6360, Jul. 2018.
[29] S. Vazquez, J. Rodriguez, M. Rivera, L. Franquelo, M. Norambuena, "Model predictive control for power converters and drives: advances and trends," *IEEE Trans. Ind. Electron.*, vol. 64, no. 2, pp. 935–947, Feb. 2017.
[30] Y. Zhang, W. Xie, Z. Li, S. Tan, and Y. Zhang, "Model predictive direct power control of a PWM rectifier with duty cycle optimization," *IEEE Trans. Power Electron.*, vol. 28, no. 11, pp. 5343–5351, Nov. 2013.
[31] K. Lee, B. Park, R. Kim, and D. Hyun, "Robust predictive current controller based on a disturbance estimator in a three-phase grid-connected inverter," *IEEE Trans. Power Electron.*, vol. 27, no. 1, pp. 276–283, Jan. 2012.
[32] A. Ahmed, B. Koh, and Y. Lee, "A comparison of finite control set and continuous control set model predictive control schemes for speed control of induction motors," *IEEE Trans. Ind. Electron.*, vol. 14, no. 4, pp. 1334–1346, Apr. 2018.
[33] C. Qi, Z. Lang, L. Su, X. Chen, and H. Miao, "Model predictive control for a bidirectional wireless power transfer system with maximum efficiency point tracking," in *Proc. IEEE Int. Symp. Predictive Control Elect. Drives Power Electron.*, 2019, pp. 1–5.
[34] C. Qi, Z. Lang, L. Su, X. Chen, and H. Miao, "Finite-control-set model predictive control for a wireless power transfer system," in *Proc. IEEE Int. Symp. Predictive Control Elect. Drives Power Electron.*, 2019, pp. 1–5.
[35] H. Li, J. Li, L. Huang, K. Wang, and X. Yang, "A novel dynamic modeling method for wireless power transfer systems," in *Proc. IEEE Appl. Power Electron. Conf. Expo.*, 2015, pp. 2740–2743.
[36] H. Hao, G. Covic, and J. Boys, "An approximate dynamic model of LCL-T-based inductive power transfer power supplies," *IEEE Trans. Power Electron.*, vol. 29, no. 10, pp. 5554–5567, Oct. 2014.
[37] S. Lee, B. Choi, and C. Rim, "Dynamics characterization of the inductive power transfer system for online electric vehicles by laplace phasor transform," *IEEE Trans. Power Electron.*, vol. 28, no. 12, pp. 5902–5909, Dec. 2013.
[38] A. Hu, "Modeling a contactless power supply using GSSA method," in *Proc. IEEE Int. Conf. Ind. Technol.*, 2009, pp. 1–6.
[39] Z. Zahid, Z. Dalala, and J. Lai, "Small-signal modeling of series-series compensated induction power transfer system," in *Proc. IEEE Appl. Power Electron. Conf. Expo.*, 2015, pp. 2847–2853.
[40] N. Bac, D. Vilathgamuwa, and U. Madawala, "A SiC-based matrix converter topology for inductive power transfer system," *IEEE Trans. Power Electron.*, vol. 29, no. 8, pp. 4029–4038, Aug. 2014.
[41] C. Choi and W. Lee, "Analysis and compensation of time delay effects in hardware-in-the-loop simulation for automotive PMSM drive system," *IEEE Trans. Ind. Electron.*, vol. 59, no. 9, pp. 3403–3410, Sep. 2012.
[42] B. Lu, X. Wu, H. Figueroa, and A. Monti, "A low-cost real-time hardware-in-the-loop testing approach of power electronics controls," *IEEE Trans. Ind. Electron.*, vol. 54, no. 2, pp. 919–931, Apr. 2007.
[43] W. Ren, M Steurer, and T. Baldwin, "Improve the stability and the accuracy of power hardware-in-the-loop simulation by selecting appropriate interface algorithms," *IEEE Trans. Ind. Appl.*, vol. 44, no. 4, pp. 1286–1294, Jul. 2008.
[44] H. Li, J. Li, K. Wang, W. Chen, and X. Yang, "A maximum efficiency point tracking control scheme for wireless power transfer systems using magnetic resonant coupling," *IEEE Trans. Power Electron.*, vol. 30, no. 7, pp. 3998–4008, Jul. 2015.
[45] Z. Huang, S. Wong, and C. K. Tse, "Control design for optimizing efficiency in inductive power transfer systems," *IEEE Trans. Power Electron.*, vol. 33, no. 5, pp. 4523–4534, May 2018.
[46] A. Berger, M. Agostinelli, S. Vesti, J. Oliver, J. Cobos, and M. Huemer, "A wireless charging system applying phase-shift and amplitude control to maximize efficiency and extractable power," *IEEE Trans. Power Electron.*, vol. 30, no. 11, pp. 6338–6348, Nov. 2015.
[47] Y. Li, J. Hu, F. Chen, Z. Li, Z. He, and R. Mai, "Dual-phase-shift control scheme with current-stress and efficiency optimization for wireless power transfer systems," *IEEE Trans. Circ. Syst. I, Reg. Papers*, vol. 65, no. 9, pp. 3110–3121, Sep. 2018.

**Shunpan Liu** received the B.S. degree in electrical engineering and automation in 2018 from the School of Electrical Engineering, Southwest Jiaotong University, Chengdu, China, where he is currently working toward the Ph.D. degree.

His main research interests include wireless power transfer, especially on control methods and circuit topology of dynamic inductive power transfer systems.

**Ruikun Mai** (Member, IEEE) received the B.Sc. and Ph.D. degrees in electrical engineering from the School of Electrical Engineering, Southwest Jiaotong University, Chengdu, China, in 2004 and 2010, respectively.

He is currently a Professor with the School of Electrical Engineering, Southwest Jiaotong University, Chengdu, China. His research interests include wireless power transfer and its application in railway systems, power system stability and control.

**Lingyun Zhou** received the B.S. degree in electrical engineering and automation in 2018 from the School of Electrical Engineering, Southwest Jiaotong University, Chengdu, China, where she is currently working toward the Ph.D. degree.

Her main research interests include wireless power transfer, especially on efficiency improvement for low-power devices.

**Yong Li** (Member, IEEE) received the B.Sc. and Ph.D. degrees from the School of Electrical Engineering, Southwest Jiaotong University, Chengdu, China, in 2013 and 2017, respectively.

From 2017 to 2018, he was a Research Associate with the Department of Electrical Engineering, The Hong Kong Polytechnic University, Hong Kong, where he was a Post-Doctoral Fellow from 2018 to 2019. He is currently an Associate Professor with Southwest Jiaotong University, Chengdu, China. His main research interests include wireless power transfer and microgrids.

**Jiefeng Hu** (Senior Member, IEEE) received the Ph.D. degree in electrical engineering from University of Technology Sydney, Ultimo, NSW, Australia, in 2013.

He was involved in the research of minigrids in Commonwealth Scientific and Industrial Research Organization, Newcastle, Australia. He was an Assistant Professor with Hong Kong Polytechnic University, Hong Kong. He is currently an Associate Professor with Federation University Australia, Ballarat, Vic, Australia. His research interests include power electronics, renewable energy, and smart microgrids.

Dr. Hu served as Committee Member and Session Chair in several international conferences, such as International Conference on Electrical Machines and System 2017 in Sydney and IET International Conference on Advanced Power System Control, Operation and Management 2018 in Hong Kong. He is an Editor of IEEE TRANSACTIONS ON ENERGY CONVERSION and a Guest Editor of IEEE TRANSACTIONS ON INDUSTRIAL ELECTRONICS for a special issue "Applications of Predictive Control in Microgrids."

**Zhengyou He** (Senior Member, IEEE) received the B.S. and M.S. degrees from Chongqing University, Chongqing, China, in 1992 and 1995, respectively, and the Ph.D. degree from Southwest Jiaotong University, Chengdu, China, in 2001.

Since 2002, he has been a Professor with the School of Electrical Engineering, Southwest Jiaotong University. He was a Visiting Scholar with Cornell University, NY, USA, from 2008 to 2009. His research interests include the area of signal processing and information theory and its application in electrical power systems, and the application of wavelet transforms in power systems

**Zhaotian Yan** received the B.Sc. degree in electrical engineering and automation in 2018 from the School of Electrical Engineering, Southwest Jiaotong University, Chengdu, China, where he is currently working toward the Ph.D. degree.

His main research interest focuses on wireless power transfer.